Electronic excitations of substitutional transition-metal ions in II-VI semiconductors: CdTe:Fe^{2+} and CdSe:Fe^{2+}

M. K. Udo, Murielle Villeret, I. Miotkowski, A. J. Mayur, A. K. Ramdas, and S. Rodriguez
Department of Physics, Purdue University, West Lafayette, Indiana 47907
(Received 30 March 1992)

The near-infrared electronic transitions of substitutional Fe^{2+} in the tetrahedral environment in the zinc-blende II-VI semiconductor CdTe and in the trigonal environment in its wurtzite counterpart CdSe are studied with Fourier-transform spectroscopy. In CdTe:Fe^{2+}, the transitions correspond to initial states in the $^5\Gamma_3$ orbital multiplet whose separation involve $\sigma=(|\lambda|/\Delta)$ and (λ^2/Δ), where λ is the spin-orbit coupling and Δ, the crystal-field splitting. The final states are sublevels of the $^5\Gamma_5$ orbital multiplet, lying Δ above $^5\Gamma_3$; their separations are in the main fixed by the magnitude of λ. The appearance and the increasing intensity of several electronic transitions, as the temperature is changed from 2.0 to $\sim$12.0 K, can be accounted for in terms of the magnetic levels which lie above the nonmagnetic Γ_1 ground state, taking into account their increasing thermal population as well as their degeneracies. The corresponding energy levels in CdTe:Fe^{2+} and CdSe:Fe^{2+} show additional splittings in the latter due to the lower trigonal symmetry. The electronic transitions in CdSe:Fe^{2+} show splittings and polarization effects associated with the trigonal symmetry. Phonon-assisted electronic transitions are observed in both CdTe:Fe^{2+} and CdSe:Fe^{2+}.

I. INTRODUCTION

In the tetrahedrally coordinated II-VI diluted magnetic semiconductors[1] (DMS) a fraction of the group-II ions are replaced by magnetic ions such as Mn^{2+}, Co^{2+}, or Fe^{2+} from the transition-metal group. The II-VI DMS's most extensively studied[1] are those in which Mn^{2+} ions are incorporated in various $A^{II}B^{VI}$ hosts, e.g., $Cd_{1-x}Mn_xTe$, $Zn_{1-x}Mn_xTe$, $Cd_{1-x}Mn_xSe$, $Zn_{1-x}Mn_xSe$, and $Hg_{1-x}Mn_xTe$. The composition ranges in which these ternary $A^{II}_{1-x}Mn_xB^{VI}$ alloys can occur in a homogeneous phase and the crystal structure they display depend on the crystal structure of the parent $A^{II}B^{VI}$ material.[1] The unique magnetic properties of Mn-based DMS alloys can be traced to the magnetic behavior of the Mn^{2+} ion, viz., (1) the interaction between the manganese spins and the spins of the conduction- and/or valence-band electrons, known as the *sp-d exchange interaction* and (2) the Mn^{2+}-Mn^{2+} *antiferromagnetic coupling* (J_{ij}) between the manganese spins. Mn-based II-VI DMS's have been intensively studied for the following reasons: (1) Mn^{2+} can be incorporated over a large composition range in the $A^{II}B^{VI}$ host without affecting its crystal structure, and (2) Mn^{2+} possesses a $^6S_{5/2}$ ground state with a very small crystal-field splitting[2] permitting a complete theoretical analysis of experimental results. Recently the interest in DMS alloys has extended to other magnetic ions besides Mn^{2+}. Bulk crystal growth of DMS's incorporating Co^{2+} and Fe^{2+} has been accomplished in a limited composition range,[3] e.g., $x \leq 0.13$ for $Cd_{1-x}Fe_xSe$. On the other hand, by using molecular-beam epitaxy (MBE), single-crystal epilayers of $Zn_{1-x}Fe_xSe$ (Ref. 4) and $Zn_{1-x}Co_xSe$ (Ref. 5) have been grown on GaAs substrates over a significantly larger composition range, viz., $0 \leq x \leq 0.22$ and $0 \leq x \leq 0.10$, respectively. There are significant differences between the electronic configurations of Mn^{2+}, Fe^{2+}, and Co^{2+} when incorporated into the II-VI semiconductors; thus the magnetic properties traced to these differences in the resulting DMS's are of considerable physical interest.

The focus of the present paper is the near-infrared transitions of Fe^{2+} in CdTe and CdSe observed at low temperatures with a Fourier transform spectrometer as a function of temperature. They are interpreted in the context of the electronic level structure calculated by Villeret, Rodriguez, and Kartheuser[6] incorporating the crystal field (tetrahedral in CdTe and trigonal in CdSe) and the spin-orbit interaction.

II. EXPERIMENTAL PROCEDURE

Single crystals of CdTe:Fe^{2+} and of CdSe:Fe^{2+} were grown by the vertical Bridgman technique[7] from presynthesized binary compounds; prior to the synthesis, Cd, Te, and Se were purified by double vacuum sublimation and Fe was outgassed in vacuum at 1050 °C; all the starting constituents are of 99.9999% purity. Single crystals with nominal concentrations of iron lower than $\sim 5\times10^{18}$ cm^{-3} were grown using a two-step procedure in which pure CdTe (CdSe) was added to single crystals of CdTe:Fe^{2+} (CdSe:Fe^{2+}) of significantly higher concentration of Fe^{2+}. Throughout the remainder of the paper only the nominal Fe^{2+} concentration of the samples is specified.

The optical surfaces of samples were prepared by grinding with carborundum of successively finer grit, followed by polishing with 3-μm diamond paste and 0.05-μm alumina. For polarization measurements on CdSe:Fe^{2+}, a crystal with wurtzite symmetry, the samples were prepared with the c axis parallel to the polished

faces.

The infrared adsorption spectra were recorded with a BOMEM DA.3 Fourier transform spectrometer[8,9] with an unapodized maximum resolution of 0.0026 cm^{-1}. In order to improve the signal-to-noise ratio each spectrum was coadded 20–50 times. Typical resolutions used in our measurements were 0.1 and 0.5 cm^{-1}, with the spectrometer operated in the vacuum mode. For the spectral range of interest a liquid-nitrogen-cooled InSb detector[10] was used. For polarization measurements an AgBr wire grid polarizer was used to select the electric vector **E** along a desired direction.

A variable-temperature stainless-steel optical cryostat[11] was used for measurements over a desired temperature range. The temperature of the sample was monitored with a calibrated thermometer installed at the sample mount and controlled by an automatic temperature controller allowing the temperature of the sample to be varied from 4.2 up to, say, 300 K, with a temperature stability of better than 0.1 K. For measurements requiring temperatures below 4.2 K, the sample chamber is first filled with liquid helium and then pumped. The optical windows of the cryostat consisted of a pair of epoxy sealed "clear tran"[12] at helium temperature (inner windows) and a pair of cesium iodide at room temperature (outer windows).

III. THEORETICAL CONSIDERATIONS

A. Energy state of Fe^{2+} in a site of tetrahedral (T_d) symmetry

The experimental results described in this paper are interpreted in terms of the energy levels of doubly ionized iron in a zinc-blende semiconductor such as CdTe where Fe^{2+} substitutes Cd^{2+} at random sites with T_d symmetry. The lowest term of the Fe^{2+} ion is ^5D; from Hund's rules the lowest level of the free ion is $^5D_4$. In a crystal field of symmetry T_d the ^5D term splits into an orbital doublet $^5\Gamma_3$ and an orbital triplet $^5\Gamma_5$. It can be shown[13] that the $^5\Gamma_3$ states lie below the orbital triplet separated by Δ, the crystal-field splitting. The spin-orbit interaction, $\lambda \mathbf{L}\cdot\mathbf{S}$, splits the 10-fold $^5\Gamma_3$ and the 15-fold $^5\Gamma_5$ multiplets as indicated on the left of Fig. 1 (see also Ref. 14). In Fe^{2+}, the strength of the spin-orbit coupling, λ, is negative. In addition it mixes the states associated with the $^5\Gamma_3$ and $^5\Gamma_5$ orbital states giving rise to corrections to the energies proportional to powers of the parameter $\sigma = |\lambda|/\Delta$. Since the operator $\lambda \mathbf{L}\cdot\mathbf{S}$ is invariant under all the operations of T_d, only states with the same symmetry can be mixed by this interaction. Therefore, it is sufficient to consider matrix elements between states belonging to identical rows of each irreducible representation reducing the problem to the diagonalization of two 3×3 and two 2×2 matrices. These have been given elsewhere[15] in connection with the study of the magnetic properties of Fe-based DMS's. We have extended the calculations of Ref. 15 to include corrections to the excited-state energies up to order σ^4. The eigenvalues obtained from perturbation calculation with σ as the small parameter are shown in Table I. An exact diagonalization of the matrices has also been performed.

B. Energy states of Fe^{2+} in a site of trigonal (C_{3v}) symmetry

In a crystal with wurtzite symmetry the tetrahedron of atoms surrounding the iron impurity is slightly distorted along the [111] direction and the site symmetry is C_{3v}. The trigonal distortion has to be included in the calculation of the energies of the levels. For this purpose it would be useful to know the strength of the trigonal distortion compared to the tetrahedral part of the crystal potential and to the spin-orbit interaction. If the trigonal field is small compared to the latter, perturbation theory is appropriate. Such an approach was used in Ref. 6. The corrections to the energies of the $^5\Gamma_3$ and $^5\Gamma_5$ states caused by the trigonal field are given in Tables VII and VIII of Ref. 6 in terms of two parameters b and c; the resulting energy levels are shown on the right in Fig. 1. Note that the ordering of the Γ_1 and Γ_3 levels originating from the two Γ_5 sublevels of $^5\Gamma_5$ multiplet of T_d is reversed with respect to that in Fig. 4 of Ref. 6. The ordering shown in Fig. 1 takes into account the experimentally determined parameters obtained in the present study. If no assumption is made regarding the relative strengths of the tetrahedral potential, the spin-orbit interaction, and the trigonal distortion, then one must diagonalize exactly the 25×25 Hamiltonian matrix. It is easily seen, from symmetry considerations, that this matrix splits into a 5×5, a 4×4, and two 8×8 submatrices corresponding to the Γ_1, Γ_2, and Γ_3 states, respectively, as shown in Ref. 16.

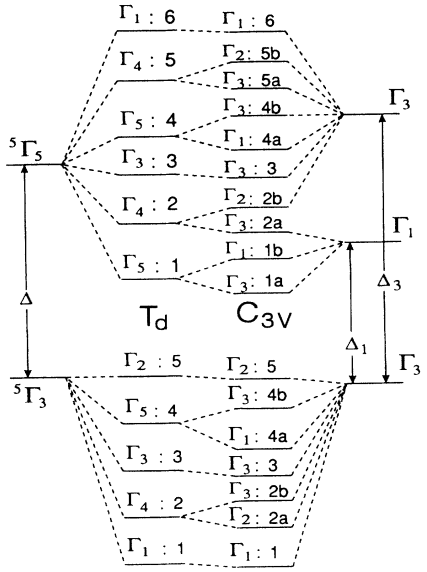

FIG. 1. Schematic diagram of the electronic energy levels of the ^5D term of Fe^{2+} in T_d and C_{3v} fields taking into account the crystal field and the spin-orbit interaction. For clarity, the energy separations in the diagram are *not* to scale. The ordering of the sublevels of Fe^{2+} in CdSe correspond to the parameters displayed in the last column of Table VII. The crystal-field splittings Δ, Δ_1, and Δ_3 are defined in Eqs. (55)–(57) in Ref. 6.

TABLE I. The energy eigenvalues of the Fe^{2+} levels corresponding to the $^5\Gamma_3$ and $^5\Gamma_5$ states. Δ is the crystal-field splitting parameter, λ is the spin-orbit coupling parameter, and $\sigma=|\lambda|/\Delta$.

Site symmetry T_d	Level	Energy eigenvalue
Γ_3	Γ_1	$(-24\lambda^2/\Delta)[1-2\sigma-20\sigma^2+\cdots]$
	Γ_4	$(-18\lambda^2/\Delta)[1-\sigma-15\sigma^2+\cdots]$
	Γ_3	$(-12\lambda^2/\Delta)[1+\sigma-11\sigma^2+\ldots]$
	Γ_5	$(-6\lambda^2/\Delta)[1+\sigma+\sigma^2+\cdots]$
	Γ_2	0
Γ_5	Γ_5	$\Delta+3\lambda+(18\lambda^2/5\Delta)[1+(63\sigma/25)+(4003\sigma^2/625)+\cdots]$
	Γ_4	$\Delta+\lambda+(6\lambda^2/\Delta)[1-3\sigma-5\sigma^2+\cdots]$
	Γ_3	$\Delta+\lambda+(12\lambda^2/\Delta)[1+\sigma-11\sigma^2+\cdots]$
	Γ_5	$\Delta-2\lambda+(12\lambda^2/5\Delta)[1-(32\sigma/25)-(4442\sigma^2/625)+\cdots]$
	Γ_4	$\Delta-2\lambda+(12\lambda^2/\Delta)[1-20\sigma^2+\cdots]$
	Γ_1	$\Delta-2\lambda+(24\lambda^2/\Delta)[1-2\sigma-20\sigma^2+\cdots]$

C. Selection rules and relative intensities of transitions

Table II shows the allowed electric dipole transitions for both T_d and C_{3v} symmetries deduced from group theory. The assignment of the experimentally observed absorption lines to the theoretically allowed transitions is complemented by a study of their intensities. A calculation of the absolute intensities of transitions requires a knowledge of the energy eigenstates including mixings with excited configurations such as $3d^5 4p$ or $3d^5 4f$, due to the odd-parity part of the crystal potential. But we content ourselves by calculating relative intensities only obtained from symmetry considerations alone. This is accomplished by making use of the theory of group representations to study the transitions between states of Fe^{2+} in a site of T_d symmetry. We first note that the transition between the $^5\Gamma_3$ and $^5\Gamma_5$ orbital states is allowed in the electric dipole approximation and that the matrix elements of the electric dipole moment operator, **d**, between initial and final states belonging to these orbital multiplets can be expressed in terms of a single parameter, since $\Gamma_5\times\Gamma_3=\Gamma_4+\Gamma_5$ contains Γ_5 only once. Following Villeret, Rodriguez and Kartheuser[14] we designate by u_i $(i=1,2)$ the Γ_3 ground-state orbital wave functions and by v_κ $(\kappa=+,0,-)$ the eigenstates of the Γ_5 orbital multiplet. These wave functions are taken to be normalized and behave as $(2z^2-x^2-y^2,\sqrt{3}(x^2-y^2))$ and $(-2^{-1/2}(x+iy),z,2^{-1/2}(x-iy))$, respectively, under the operations of T_d. Here x, y, and z are projections of the position vector **r** on the cubic axes of the crystal. The combinations of the components of **d** and the functions u_1,u_2 belonging to Γ_4 and Γ_5 are obtained from the Clebsch-Gordan coefficients for T_d. These allow us to express the matrix elements of **d** between u_i and v_κ in terms of a single parameter, say d_0. They are

$$\langle v_\kappa|\mathbf{d}|u_i\rangle=\frac{d_0}{2}\begin{bmatrix} 2^{-1/2}(\hat{\mathbf{x}}-i\hat{\mathbf{y}}) & -(\tfrac{3}{2})^{1/2}(\hat{\mathbf{x}}+i\hat{\mathbf{y}}) \\ 2\hat{\mathbf{z}} & 0 \\ -2^{-1/2}(\hat{\mathbf{x}}+i\hat{\mathbf{y}}) & (\tfrac{3}{2})^{1/2}(\hat{\mathbf{x}}-i\hat{\mathbf{y}}) \end{bmatrix}. \quad (1)$$

The total intensity of the electric dipole transition from $^5\Gamma_3$ to $^5\Gamma_5$ in the absence of the spin-orbit interaction is obtained from Eq. (1) adding the squares of the magnitudes of the matrix elements incoherently and multiplying by the spin degeneracy to yield $I_0=15|d_0|^2$. We calculate the intensities of transitions between the spin-orbit-split states in terms of d_0, using Eq. (1) and the wave functions for the spin-orbit-split levels given in Tables VI and VIII of Ref. 14. The relative intensities are obtained dividing the calculated matrix elements, properly squared, by I_0. The results are displayed in Table III; for transitions between degenerate states, the squares of the magnitudes of the matrix elements of **d** are added incoherently.

TABLE II. Selection rules for electric dipole transitions showing the allowed transitions for both T_d and C_{3v} site symmetries.

T_d		C_{3v}		
Initial state	Final state	Initial state		Final state
			E‖c	E⊥c
Γ_1	Γ_5	Γ_1	Γ_1	Γ_3
Γ_2	Γ_4	Γ_2	Γ_2	Γ_3
Γ_3	Γ_4,Γ_5	Γ_3	Γ_3	$\Gamma_1,\Gamma_2,\Gamma_3$
Γ_4	$\Gamma_2,\Gamma_3,\Gamma_4,\Gamma_5$			
Γ_5	$\Gamma_1,\Gamma_3,\Gamma_4,\Gamma_5$			

IV. EXPERIMENTAL RESULTS

A. CdTe:Fe^{2+}

Figure 2 shows the optical-absorption spectrum of Fe^{2+} in CdTe at the temperature $T=5.7$ K and $n(Fe^{2+})$, the concentration of Fe^{2+}, of 5×10^{17} cm^{-3}. In addition to the very strong and sharp absorption lines between 2250 and 2300 cm^{-1}, several additional weak and broad features appear at higher wave numbers. We first focus on the features labeled $X_{\rm I}, Y, {\rm I}, {\rm II}, \ldots$. As the temperature is raised in small increments, from 2.0 to 8.8 K (see Fig. 3), I and $X_{\rm I}$ become broader, whereas II in-

TABLE III. The normalized relative intensity of the allowed electronic transitions of Fe^{2+} in CdTe. According to the energy diagram shown in Fig. 1, the allowed transitions are labeled as $(A \rightarrow B)$, where A and B are shown after the colon in the designation of the irreducible representations of each energy level, i.e., $A = 1,2,3,4,5$ and $B = 1,2,3,4,5,6$.

Allowed transition	Label	Relative intensity	Allowed transition	Label	Relative intensity
$(1\rightarrow1)$	I	$\frac{1}{25}$	$(4\rightarrow1)$	IV	$\frac{3}{100}$
$(1\rightarrow4)$		$\frac{3}{50}$	$(4\rightarrow2)$		$\frac{1}{60}$
$(2\rightarrow1)$	II	$\frac{9}{100}$	$(4\rightarrow3)$		$\frac{2}{15}$
$(2\rightarrow2)$		$\frac{1}{20}$	$(4\rightarrow4)$		$\frac{1}{50}$
$(2\rightarrow3)$		0	$(4\rightarrow5)$		$\frac{1}{30}$
$(2\rightarrow4)$		$\frac{3}{50}$	$(4\rightarrow6)$		$\frac{1}{15}$
$(2\rightarrow5)$		$\frac{1}{10}$	$(5\rightarrow2)$		$\frac{1}{15}$
$(3\rightarrow1)$	III	$\frac{1}{25}$	$(5\rightarrow5)$		$\frac{1}{30}$
$(3\rightarrow2)$		$\frac{1}{15}$			
$(3\rightarrow4)$		$\frac{3}{50}$			
$(3\rightarrow5)$		$\frac{1}{30}$			

creases in intensity significantly and broadens above 8.8 K; Y is noticeably broader than the other lines at all temperatures. The behavior of II is a clear signature of a transition originating from a level lying above the ground state, but separated from it by a small energy; its initial state is thus increasingly populated with increasing temperature. The temperature dependence of II is further illustrated in Fig. 4, where the results on a sample with a higher concentration of Fe^{2+} are displayed; II is significantly stronger, consistent with the higher concentration of Fe^{2+} and its striking temperature dependence is again clearly evident. Figures 3 and 4 also show the temperature and concentration dependence of X_{II}, similar to that of II, again indicating a transition originating from a level lying above the ground state. However, X_{II} is not as sharp as II reflecting its association with X_I, as will be discussed later. Additional lines III and IV are also observed in this sample. Figure 3(a) shows the transmission spectrum at $T = 2.0$ K. Lines I, X_I, and Y remain very strong, but lines II, X_{II}, III, and IV, present in Fig. 4, are now obliterated. The absence of these lines at 2.0 K, strongly corroborates the assignments for II, III, and IV in which the initial states are the higher-lying levels of the split orbital ground state $^5\Gamma_3$.

In Table IV, column 3, we list the experimental values for the energies of lines I–IV and the assignments based on their temperature and concentration dependence, interpreted in the context of the theoretical calculations. In column 4 we list the values obtained from the perturbation results of Table I whereas those obtained from an exact diagonalization of the Hamiltonian are listed in column 5. Following the energy diagram shown in Fig. 1, we label the transitions as $(A \rightarrow B)$, where A and B are shown after the colon in the designation of the irreducible representations of each energy level, i.e., $A = 1,2,3,4,5$ and $B = 1,2,3,4,5,6$.

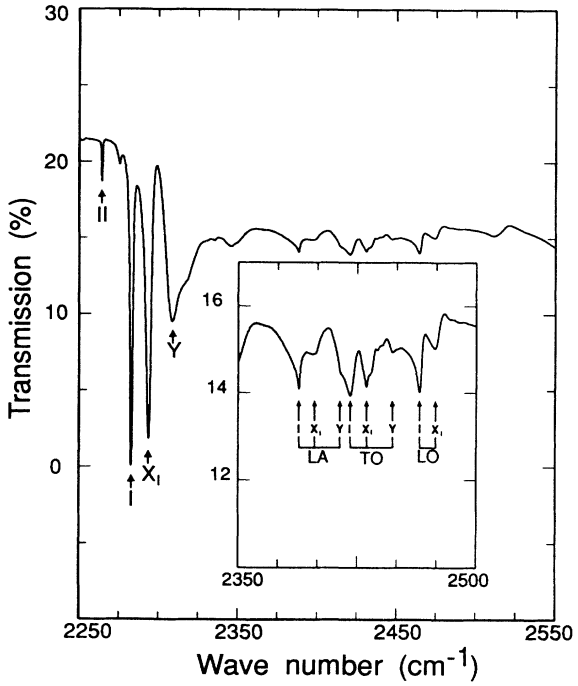

FIG. 2. Transmission spectrum of Fe^{2+} in CdTe with Fe^{2+} concentration, $n(Fe^{2+}) = 5\times10^{17}$ cm^{-3}, sample thickness $t = 0.291$ cm, and temperature $T = 5.7$ K. The various electronic transitions are labeled I, II, X_I, and Y. The vertical scale in the inset has been expanded in order to highlight the various phonon assisted transitions which are indicated by the vertical arrows: LA, TO, and LO are the phonons involved with the electronic transitions I, X_I and Y.

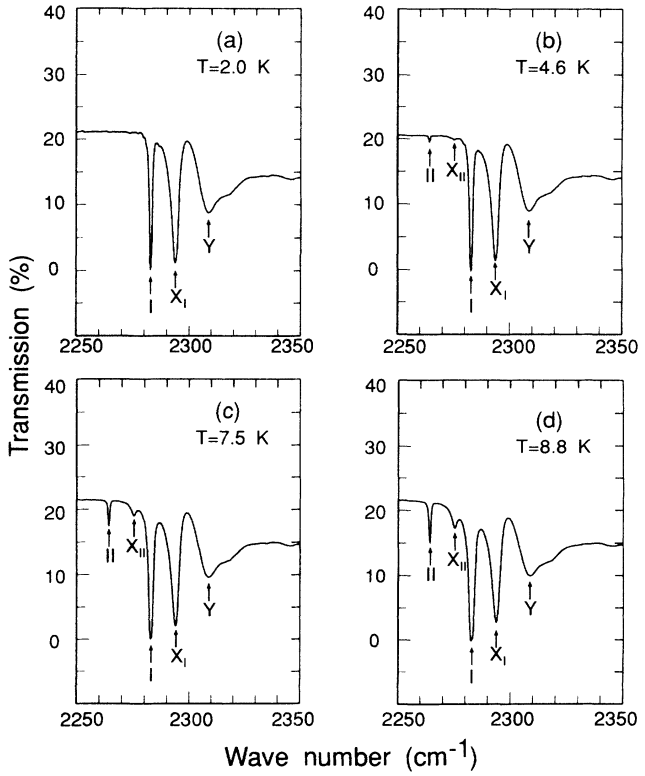

FIG. 3. Transmission spectra of Fe^{2+} in CdTe with $n(Fe^{2+}) = 5\times10^{17}$ cm^{-3}, $t = 0.291$ cm, and (a) $T = 2.0$ K, (b) $T = 4.6$ K, (c) $T = 7.5$ K, and (d) $T = 8.8$ K.

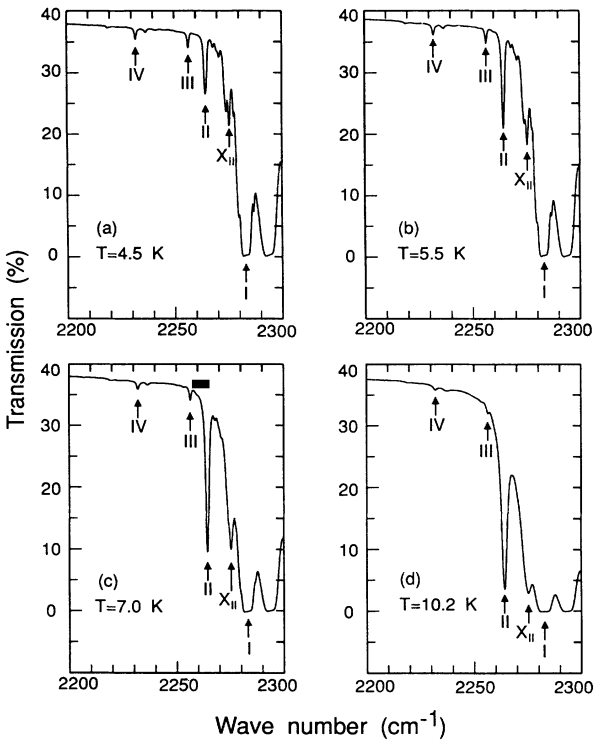

FIG. 4. Transmission spectra of Fe^{2+} in CdTe with $n(Fe^{2+})=5\times10^{18}$ cm^{-3}, $t=0.160$ cm, and (a) $T=4.5$ K, (b) $T=5.5$ K, (c) $T=7.0$ K, and (d) $T=10.2$ K. Additional electronic transitions III and IV are observed in these spectra.

We compare the relative intensities of I, II, and III at 4.5 K predicted from Table III and observed in Fig. 4 by taking due account of the Boltzmann factor, $\exp(-\Delta E/k_BT)$, controlling the thermal population of Γ_4:2 and Γ_3:3 levels of the $^5\Gamma_3$ multiplet. The intensities of I, II, and III were determined by calculating the area under the curve representing absorption coefficient versus wave number. For line I a curve fitting was necessary due to its strong absorption leading to almost zero transmission close to the peak position. The experimental value for the ratio of the intensities of I and II $=1.1\times10^2$; of I and III $=4.3\times10^3$; and of II and III $=38.0$, while theoretically these ratios are expected to be 1.9×10^2, 5.4×10^3, and 28.4, respectively. The experimental results and the theoretical values are in reasonable agreement.

The transition from the Γ_1:1 ground state to the Γ_5:4 excited state should also appear at the lowest temperature for the same reason as does line I and with comparable intensity as can be seen from Table III. It should appear at an energy $\sim5\lambda$ above that of line I. We have made a search for this transition ~2800 cm^{-1} but failed to observe any indication of it. Its absence is puzzling. We note that Baranowski, Allen, and Pearson[19] also did not report any feature in this energy range which could be ascribed to this transition [see Fig. 1(c) in their paper].

The origin of X_I, X_{II}, and Y is not yet clear. X_I and Y appear in conjunction with I, at *all* temperatures, indicating that they too originate from a ground state. According to Fig. 1, at the lowest temperature, with Γ_1:1 alone populated, only Γ_1:1$\rightarrow\Gamma_5$:1 and Γ_1:1$\rightarrow\Gamma_5$:4 are expected to appear in the absorption spectrum, but with a separation of $\sim5\lambda$, λ being the spin-orbit coupling parameter. As shown in Table IV, we ascribe I to Γ_1:1$\rightarrow\Gamma_5$:1, thus allowing no assignments for X_I, X_{II}, and Y consistent with the energy level scheme; Γ_1:1$\rightarrow\Gamma_5$:4 should be separated from I by ~500 cm^{-1} with $|\lambda|\sim100$ cm^{-1}. Thus X_I, X_{II}, and Y do not appear to be associated with an isolated Fe^{2+} ion. It is therefore of interest to explore if they could arise from Fe^{2+} complexes such as pairs of Fe^{2+}.

The Hamiltonian of an Fe^{2+}-Fe^{2+} pair can be written as the sum of two Hamiltonians of the form given in Eq. (1), Ref. 6, one for each of the ions plus a term expressing the antiferromagnetic exchange interaction between the two ions. The Fe^{2+}-Fe^{2+} pair wave function is then taken as a linear combination of products of the single-ion wave functions. A detailed picture of the energy levels associated with the Fe^{2+} pairs in CdTe requires the diagonalization of a 625×625 matrix corresponding to $^5\Gamma_3\times{}^5\Gamma_3$, $^5\Gamma_5\times{}^5\Gamma_3$, $^5\Gamma_3\times{}^5\Gamma_5$, and $^5\Gamma_5\times{}^5\Gamma_5$. In the absence of exchange interaction, the levels arising from $^5\Gamma_3\times{}^5\Gamma_5$ and $^5\Gamma_5\times{}^5\Gamma_3$ are degenerate and separated

TABLE IV. The near-infrared absorption lines of Fe^{2+} in CdTe. The assignment of the observed transitions follows the nomenclature ($A\rightarrow B$), where A is one of the levels of the split orbital ground state $^5\Gamma_3$ and B is one of the levels of $^5\Gamma_5$ excited orbital state, as illustrated in the energy level diagram depicted in Fig. 1. The theoretical values were calculated using $\Delta=2470$ cm^{-1} and $\lambda=-91$ cm^{-1}. (Δ and λ were selected in order to achieve the best fit between the experimental data and the theoretically calculated values for the energies of the various transitions.)

Line no.	Assignment	Experimental values (cm^{-1})	Calculated values (cm^{-1}) Perturbation theory	Exact
I	(1→1)	2282.8	2282.6	2283.2
II	(2→1)	2264.1	2267.2	2267.3
III	(3→1)	2256.3	2251.4	2251.3
IV	(4→1)	2231.9	2231.2	2231.1
X_I	Fe^{2+} complex	2293.8		
X_{II}	Fe^{2+} complex	2275.1		
Y	Fe^{2+} complex	2309.0		

from the ground orbital states $^5\Gamma_3 \times {}^5\Gamma_3$ by Δ, equal to the crystal-field splitting in the single ion. The exchange interaction removes this degeneracy causing shifts of the order of $2J_{NN}$, the constant defining the antiferromagnetic coupling of nearest neighbors (NN), typically ~ 10 cm^{-1} in the diluted magnetic semiconductors.[17] The Fe^{2+}-Fe^{2+} antiferromagnetic interaction may be visualized to arise in a manner not unlike the van der Waals interaction between spherically symmetric noble-gas atoms. Analogous to the virtual excitations to p states resulting in fluctuating electric dipole moment of each noble-gas atom, interaction between the two nonmagnetic Fe^{2+} ions could have their origin in fluctuations in the magnetic dipole moment of one causing a similar fluctuation in the other. This model needs to be explored quantitatively. The levels $^5\Gamma_5 \times {}^5\Gamma_5$ lie at an energy 2Δ above the orbital ground states. The exchange interaction is much smaller than Δ and in first approximation we can infer that transitions between the ground state and the excited states of the Fe^{2+} pair will occur at energies close to those for the single Fe^{2+} ions. The energies associated with X_I and Y are 2293.8 and 2309.0 cm^{-1}, respectively. From the argument presented above for the Fe^{2+}-Fe^{2+} pairs, we tentatively attribute X_I, X_{II} and Y to electronic transitions associated with complexes such as pairs of Fe^{2+} in CdTe. More specifically, one could identify X_I and X_{II} as the counterparts of I and II of isolated Fe^{2+} in an Fe^{2+} complex, viz., as transitions originating from a ground state of an Fe^{2+} complex and a level lying above this ground state and terminating in a common final state, with X_{II} disappearing at the lowest temperatures. For a sample with $n(Fe^{2+})=1.3\times10^{17}$ cm^{-3}, Fig. 5(a) shows the dramatic decrease of X_I and the disappearance of Y, while I remains distinctly visible, with an intensity consistent with the lower concentration of Fe^{2+}. This result indicates that X_I and Y are related to Fe^{2+} complexes and not to single Fe^{2+} ions.

We now turn our attention to the various broad and weak absorption features occurring for wave numbers larger than ~ 2300 cm^{-1} (Fig. 2). These absorption features are present even at the lowest temperatures indicating that they are related to I, X_I, and Y. A close inspection reveals that the energies of the weak absorption features exceed those of I, X_I, and Y by fixed values, consistent with the phonon energies of CdTe. We therefore ascribe these weak absorption features to phonon-assisted transitions, as already pointed out by Slack and coworkers.[18,19] We list in Table V the various phonons occurring in CdTe at the center of the Brillouin zone, at the Γ point, as well as at zone boundaries, L and X points. The observation of these zone boundary phonons in CdTe has been attributed to impurities (intentionally or unintentionally introduced in the crystal) and also to the naturally occurring isotopes in the DMS which act as simple mass defects. We note here that the experimental data for phonons at the zone boundary are somewhat sparse. The energies of the various observed phonon-assisted electronic transitions in Fig. 2 are tabulated in Table VI. The calculated values in Table VI, obtained by adding the phonon energies listed in Table V to the experimentally observed energies of lines I, X_I, and Y are in good agreement with the experimental values.

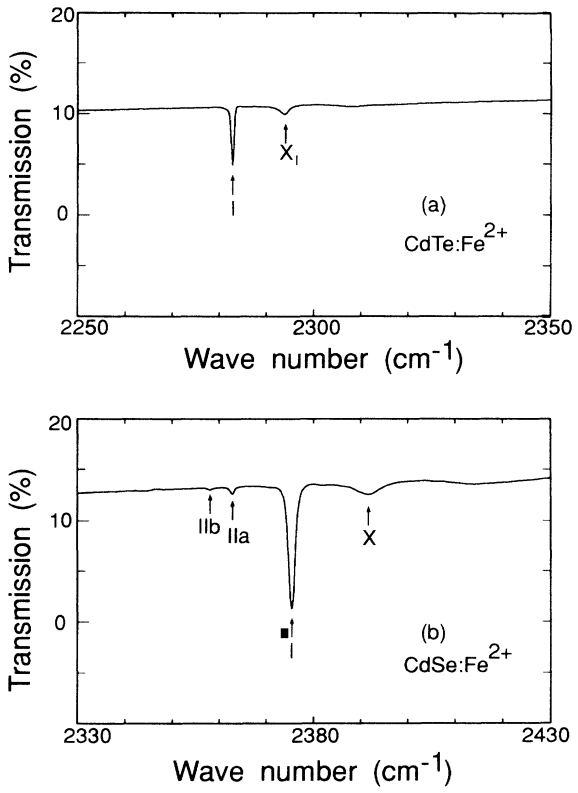

FIG. 5. Transmission spectra of Fe^{2+} in (a) CdTe with $n(Fe^{2+})=1.3\times10^{17}$ cm^{-3}, $t=0.220$ cm, $T=4.9$ K, and (b) CdSe with $n(Fe^{2+})=1.0\times10^{17}$ cm^{-3}, $t=0.126$ cm, and $T=5.1$ K.

Finally, we record an unusual splitting exhibited by line II as the temperature is lowered from 4.9 to 2.0 K shown in Fig. 6. A similar behavior is observed for X_{II}. The absence of such a splitting for I indicates that it must be associated with the initial state of II, i.e., Γ_4. Whether this effect is associated with a Jahn-Teller distortion needs to be established with further experiments.

TABLE V. Phonon energies for CdTe in cm^{-1}.

Assignment	a	b	c	d	e
LO(Γ)	169.3		171.0	180.0	173
TO(Γ)	140.0		140.0	140.0	147
LO(L)	144.3				
TO(L)	144.3				
LA(L)	108.3	104.5		105.0	
TA(L)	29.3	36.0		65.0	
TO(X)	148.7				
TA(X)	35.0	46.0			

[a]Rowe *et al.* (Ref. 20).
[b]Slack, Roberts and Vallin (Ref. 19).
[c]Mooradian and Wright (Ref. 21).
[d]Slack, Ham, and Chrenko (Ref. 18).
[e]Peterson (Ref. 22).

TABLE VI. Phonon-assisted transition of Fe^{2+} in CdTe.

Experimental values (cm^{-1})	Assignment	Calculated values (cm^{-1}) a	b	c
2388.3	I+LA	2391.1	2387.8	
2398.1	X_I+LA	2402.1	2398.8	
2414.1	Y+LA	2417.3	2414.0	
2420.7	I+TO	2422.8	2422.8	2429.8
2430.9	X_I+TO	2433.8	2433.8	2440.8
2447.6	Y+TO	2449.0	2449.0	2456.0
2464.5	I+LO	2452.1	2462.8	2455.8
2474.7	X_I+LO	2463.1	2473.8	2466.8

[a]Rowe *et al.* (Ref. 20).
[b]Slack, Ham, and Chrenko (Ref. 18).
[c]Peterson (Ref. 22).

B. CdSe:Fe^{2+}

The optical-absorption spectrum of Fe^{2+} in CdSe at 4.5 K with $n(Fe^{2+})=5\times10^{18}$ cm^{-3} is displayed in Fig. 7. A close resemblance between Figs. 2 and 7 is immediately evident. Following the notation used for Fe^{2+} with T_d site symmetry, here we also label the sharp lines as *X*, *Y*, I, II, and so on. In order to keep the labeling of the optical transitions for both tetrahedral and trigonal fields consistent, we use the following notation: (a) the energy levels which do not undergo further splitting under trigonal field have the same label for both T_d and C_{3v}; (b) the levels which split under the trigonal crystal field are labeled by a number indicating the original tetrahedral level to which it is correlated (e.g., 1,2,3,...) followed by a letter according to the number of split levels (e.g., *a*,*b*,*c*,...). For example, in Fig. 1 for C_{3v}, the transitions $(1\rightarrow1a)$ and $(1\rightarrow1b)$ correspond to those with Γ_1 of the orbital multiplet $^5\Gamma_3$ as the initial state and the lowest $\Gamma_3(C_{3v})$ and $\Gamma_1(C_{3v})$ of the excited multiplet $^5\Gamma_5$ as the final states.

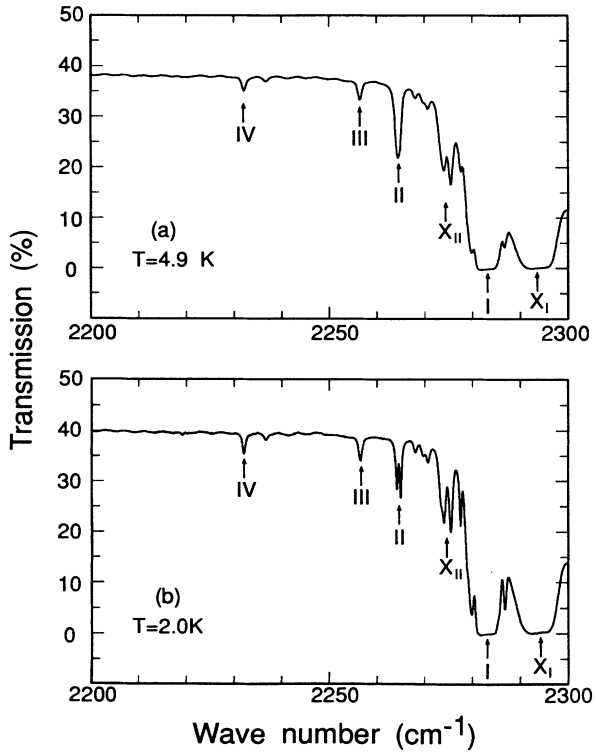

FIG. 6. Transmission spectra of Fe^{2+} in CdTe with $n(Fe^{2+})=1.0\times10^{19}$ cm^{-3}, $t=0.195$ cm, and (a) $T=4.9$ K, and (b) $T=2.0$ K.

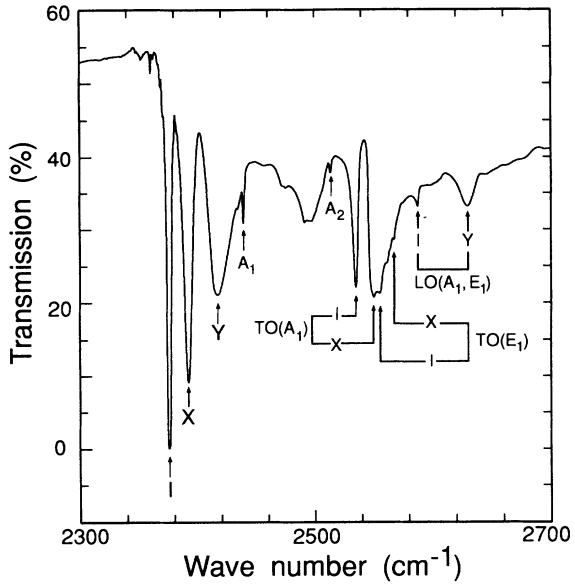

FIG. 7. Transmission spectrum of Fe^{2+} in CdSe with $n(Fe^{2+})=5\times10^{18}$ cm^{-3}, $t=0.060$ cm, and $T=2.0$ K. In addition to the electronic transitions I, *X*, and *Y*, phonon-assisted transitions are identified as combinations of LO or TO phonons with I, *X*, or *Y*.

Figure 8 shows the temperature dependence of I, IIa, IIb, *X*, and *Y*. There is a dramatic increase in absorption for lines IIa and IIb as the temperature changes from 2.0 to 8.1 K; further increase in temperature broadens the lines. The temperature dependence of IIa and IIb indicates that they could correspond to electronic transitions originating from Γ_2:2*a* and Γ_3:2*b* and terminating at Γ_3:1*a* or Γ_1:1*b*. The absence of IIa and IIb in the spectrum at 2.0 K, shown in Fig. 8(a), confirms that their initial states lie above Γ_1:1. The selection rules for the allowed transitions of Fe^{2+} for C_{3v} site symmetry are $\Gamma_1\rightarrow\Gamma_1$, $\Gamma_2\rightarrow\Gamma_2$, and $\Gamma_3\rightarrow\Gamma_3$ for E||c, and $\Gamma_1\rightarrow\Gamma_3$, $\Gamma_2\rightarrow\Gamma_3$, and $\Gamma_3\rightarrow\Gamma_1,\Gamma_2,\Gamma_3$ for E⊥c. Polarization measurements, with E parallel and perpendicular to c, are presented in Fig. 9. The occurrence of I at the same energy for both E||c and E⊥c implies that the lowest states Γ_3:1*a* and Γ_1:1*b* of the orbital multiplet $^5\Gamma_5$ are coincident within the resolution of the experiment. Similarly IIb can be ascribed to Γ_3:2*b*$\rightarrow\Gamma_1$:1*b* expected for E⊥c and Γ_3:2*b*$\rightarrow\Gamma_3$:1*a*, expected for E⊥c and E||c, respectively, the coincidence of the final-state energies resulting in a single line as in the case of I. The values of λ, Δ, *b*, and *c* are obtained from the positions of the experimentally observed transitions I, IIa, and IIb, taken together with the coincidence of the final states Γ_1 and Γ_3. These parameters obtained from the data are displayed in Table VII us-

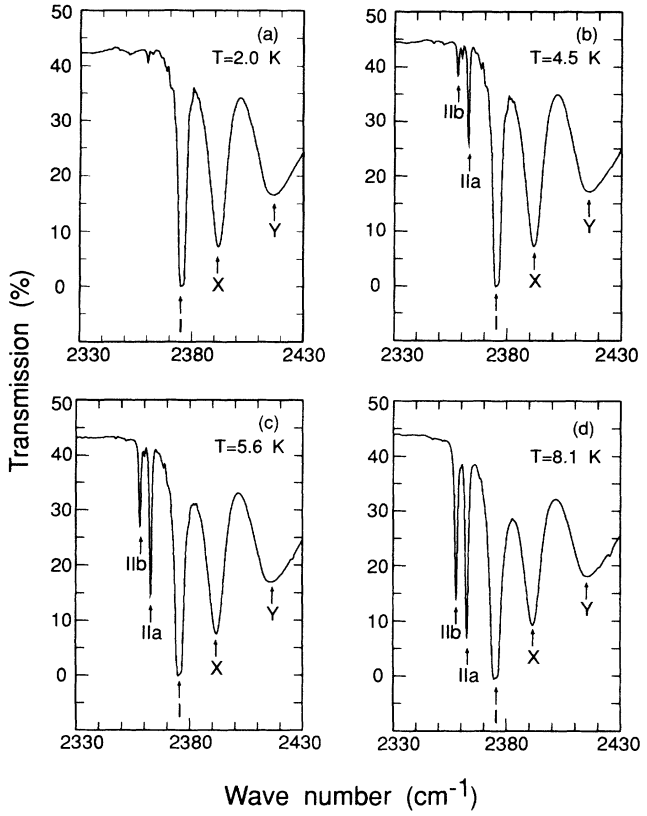

FIG. 8. Transmission spectra of Fe^{2+} in CdSe with $n(Fe^{2+})=5\times10^{18}$ cm^{-3}, $t=0.060$ cm, and (a) $T=2.0$ K, (b) $T=4.5$ K, (c) $T=5.6$ K, and (d) $T=8.1$ K.

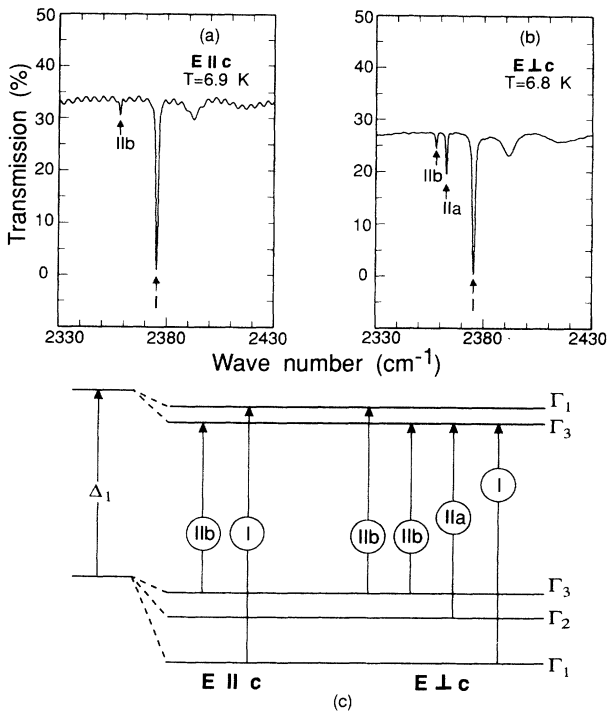

FIG. 9. Transmission spectra of Fe^{2+} in CdSe with $n(Fe^{2+})=5.1\times10^{17}$ cm^{-3}: (a) $\mathbf{E}\|\mathbf{c}$, $T=6.9$ K; (b) $\mathbf{E}\perp\mathbf{c}$, $T=6.8$ K; and (c) the initial and final states for I, IIa, and IIb.

ing the perturbation theory and the exact diagonalization. We note that the parameters were initially obtained using the perturbation theory and subsequently refined in the exact diagonalization procedure.

In the context of the above observations the electronic Raman studies of Scalbert *et al.*[23] on CdSe:Fe^{2+} are of particular interest; they reported Raman lines at 13.0 and 17.6 cm^{-1} and assigned them to transitions *within* the orbital multiplet $^5\Gamma_3$, more specifically (in the present notation) to the transitions $\Gamma_1{:}1\rightarrow\Gamma_2{:}2a$ and $\Gamma_1{:}1\rightarrow\Gamma_3{:}2b$, respectively. Note that the irreducible representations Γ_1, Γ_2, and Γ_3 of C_{3v}, the site symmetry of Fe^{2+} in the wurtzite structure, are also labeled in the literature as A_1, A_2, and E, respectively.[24] The Raman tensors relevant in the two transitions observed transform as $\Gamma_2(A_2)$ and $\Gamma_3(E)$. The Raman tensor belonging to $\Gamma_2(A_2)$ is entirely antisymmetric whereas that transforming as $\Gamma_3(E)$ has both symmetric and antisymmetric components. They are

$$\alpha(\Gamma_1\rightarrow\Gamma_2):\begin{bmatrix}0 & t & 0\\ -t & 0 & 0\\ 0 & 0 & 0\end{bmatrix}, \tag{2}$$

$$\alpha(\Gamma_1\rightarrow\Gamma_3(X)):\begin{bmatrix}r & 0 & s\\ 0 & -r & 0\\ s & 0 & 0\end{bmatrix}+\begin{bmatrix}0 & 0 & -u\\ 0 & 0 & 0\\ u & 0 & 0\end{bmatrix}, \tag{3}$$

TABLE VII. The near-infrared optical absorption lines of Fe^{2+} in CdSe. The assignment of the observed transitions follows the nomenclature ($A\rightarrow B$), where A is one of the levels of the ground multiplet Γ_3 and B is the lowest state of the excited multiplet Γ_1. Also listed are the strength of the crystal-field parameters Δ, b, and c as well as that of the spin-orbit coupling, λ.

Line no.	Experimental values (cm^{-1})	Assignment		Perturbation theory (cm^{-1})	Exact theory (cm^{-1})
I	2375.4	$(1\rightarrow1a)+(1\rightarrow1b)$	Δ	2546.1	2550.6
IIa	2362.8	$(2a\rightarrow1a)$	λ	−93.3	−94.0
IIb	2358.0	$(2b\rightarrow1a)+(2b\rightarrow1b)$	b	12.5	28.0
			c	−28.1	−22.0
X	2391.8	Fe^{2+} complex			
Y	2416.4	Fe^{2+} complex			

$$\alpha(\Gamma_1 \rightarrow \Gamma_3(Y)): \begin{bmatrix} 0 & -r & 0 \\ -r & 0 & s \\ 0 & s & 0 \end{bmatrix} + \begin{bmatrix} 0 & 0 & 0 \\ 0 & 0 & -u \\ 0 & u & 0 \end{bmatrix} . \quad (4)$$

The tensors are referred to an orthogonal coordinate axes **x**,**y**,**z** with **z**$\|$**c** and **y** normal to one of the reflection planes σ_v.

One of the scattering geometries employed by Scalbert *et al.*[23] involves backscattering normal to **c** (Fig. 3 of Ref. 23). The authors have not specified if the incident light propagates along **x** or **y** in the backscattering geometry. Also it is not clear if the incident light is polarized and the scattered light is analyzed. However it can be easily shown that the $\Gamma_1 \rightarrow \Gamma_2$ line at 13.0 cm^{-1} is forbidden in (yy), (yz), (zy), and (zz) polarizations if the incident light is along **x** as well as in (xx), (xz), (zx), and (zz) polarizations if it is along **y**. Thus the observation of the 13.0-cm^{-1} line in the backscattering geometry may be due to the resonance conditions under which the spectrum was recorded. The $\Gamma_1 \rightarrow \Gamma_3$ line at 17.6 cm^{-1} is expected in (yy), (yz), and (zy) as well as in (xx), (xz), and (zx) polarizations. Its absence in the spectrum is presumably due to its low intensity.

The results for 90° scattering presented in Fig. 2 of Ref. 23 involve scattered radiation along **c** and incident radiation polarized either parallel or perpendicular to it. Again, in the absence of the specification of the direction of incidence and the polarization of the scattered light, one can anticipate the appearance of $\Gamma_1 \rightarrow \Gamma_2$ in (xy) and (yx) polarizations accessible for incident light polarized perpendicular to **c**; the spectrum in Fig. 2(b) confirms this prediction. However, the observation of the $\Gamma_1 \rightarrow \Gamma_2$ in Fig. 2(a), i.e., for incident light polarized along **c**, represents a contradiction since it is forbidden in (zx) or (zy). The appearance of $\Gamma_1 \rightarrow \Gamma_3$ in both Figs. 2(a) and 2(b) is entirely consistent with the selection rules allowing it in (xx), (xy), (zx), and (zy) or (yy), (yx), (zy), and (zx) polarization configurations.

In the far infrared, electric dipole selection rules allow $\Gamma_1{:}1 \rightarrow \Gamma_3{:}2b$ in **E**$\perp$**c** only and forbid $\Gamma_1{:}1 \rightarrow \Gamma_2{:}2a$ in both **E**$\|$**c** and **E**$\perp$**c**. However, the energies of these transitions can be deduced from the positions of the near-infrared transitions $\Gamma_1{:}1 \rightarrow \Gamma_3{:}1a$ (line I), $\Gamma_2{:}2a \rightarrow \Gamma_3{:}1a$ (line IIa), and $\Gamma_3{:}2b \rightarrow \Gamma_3{:}1a$ (line IIb), viz., 12.6$\pm$0.1 cm^{-1} for the energy separation between $\Gamma_1{:}1$ and $\Gamma_2{:}2a$ and 17.2$\pm$0.1 cm^{-1} for the energy separation between $\Gamma_1{:}1$ and $\Gamma_3{:}2b$ of the ${}^5\Gamma_3$ orbital multiplet, in good agreement with the Raman data.

We note that, besides I, *X*, and *Y*, other features observed at higher wave numbers, remain strong at the lowest temperatures. Following the analogous behavior of the corresponding lines *X* and *Y* in CdTe:Fe^{2+}, we attribute them also to antiferromagnetically coupled Fe^{2+} complexes. The striking decrease in the intensity of *X* relative to that of I and the absence of *Y* in Fig. 5(b) for a sample with $n(Fe^{2+}) = 1 \times 10^{17}$ cm^{-3}, as compared to the results in Fig. 8 for a concentration of 5×10^{18} cm^{-3}, support this interpretation.

As in CdTe:Fe^{2+}, absorption features occur in CdSe:Fe^{2+} in the energy range expected for electronic transitions in combination with phonons. In CdSe some of these features are sharp and intense. In Table VIII we list the zone center phonons observed in CdSe; phonon energies for other points of the Brillouin zone have not been reported in the literature. Figure 7 displays the various features attributed to phonon assisted transitions and their energies are listed in Table IX; in the table we also list the energies of I, *X*, and *Y* in combination with the various zone center phonons. A fair agreement is observed between the experimental and the calculated energies for these phonon-assisted transitions. The lines A_1(2438.7 cm^{-1}) and A_2(2513.2 cm^{-1}) occur at energies consistent with acoustic-phonon-assisted transitions; however, the lack of experimental data for such phonons prevents an unambiguous identification for these transitions.

V. CONCLUDING REMARKS

The present study in conjunction with the theoretical calculations has provided the identification and ordering of the transitions from the sublevels of the ground-state orbital to those of the first excited orbital, both having experienced a crystal-field splitting. In this context, far infrared measurements are of interest as they will enable the observation of transitions within the ground-state multiplet directly. The observations reported in this paper provide an unambiguous evidence for the energy-level splitting associated with the trigonal (C_{3v}) symmetry in the wurtzite structure, as opposed to the tetrahedral (T_d) symmetry in the zinc-blende structure of the host in which Fe^{2+} has been incorporated. It is of interest to note that the lowest state of Fe^{2+} is nonmagnetic and the magnetism of Fe-based DMS is an example of Van Vleck paramagnetism, in which a mixing of the higher-lying states with the lowest state is observed in the presence of a magnetic field. This problem has been explored in detail by Villeret, Rodriguez, and Kartheuser[15] who emphasized the anisotropy of the Van Vleck paramagnetism of even the cubic CdTe:Fe^{2+}; in CdSe:Fe^{2+} the anisotropy is in the main related to the trigonal symmetry and the associated energy-level splitting. Villeret, Rodriguez, and Kartheuser[16] have also made a comprehensive study of the magnetic-field splitting and shifts of Fe^{2+} in DMS. The results of polarization measurements on CdSe:Fe^{2+} indicate the coincidence of the lowest levels Γ_1 and Γ_3 of the excited multiplet, $\Gamma_1{:}1b$ and $\Gamma_3{:}1a$ in Fig. 1, thus yielding an additional constraint in the parameters involved in the theoretical calculations.

TABLE VIII. Phonons in CdSe in cm^{-1}.

Assignment	a	b
LO(Γ, A_1)	213	
TO(Γ, A_1)	169	
LO(Γ, E_1)	214	
TO(Γ, E_1)	174	
TA(A_3)		43.5

[a]Suh *et al.* (Ref. 25).
[b]Beserman (Ref. 26).

TABLE IX. Phonon-assisted transitions of Fe^{2+} in CdSe at low temperatures.

Experimental values (cm^{-1})	Assignment	Calculated values[a] (cm^{-1})
2438.7		
2513.2		
2534.8	$I+TO(A_1)$	2544.4
2550.2	$X+TO(A_1)$	2560.8
2555.3	$I+TO(E_1)$	2549.4
2567.4	$X+TO(E_1)$	2565.8
2587.5	$I+LO(A_1)$	2588.4
	$I+LO(E_1)$	2589.4
2629.6	$Y+LO(A_1)$	2629.4
	$Y+LO(E_1)$	2630.4

[a]Suh *et al.* (Ref. 25).

Besides Fe-based II-VI DMS, other diluted magnetic semiconductors are worthy of study in view of the similarities and differences in the electronic level structure of the different transition-metal ions. Co^{2+} as well as Cu^{2+} have an odd number of electrons, by Kramers's theorem, all their eigenstates have even degeneracies and thus must always exhibit paramagnetism. Fe^{2+} and Ni^{2+}, on the other hand, have an even number of electrons and can have both degenerate and nondegenerate states. It turns out that in the crystals under study, the ground states of Fe^{2+} and Ni^{2+} are nondegenerate and, in the first approximation, are nonmagnetic but can exhibit Van Vleck paramagnetism because of magnetic excited states which are separated by small energies. Thus DMS based on Ni^{2+} will provide a case analogous to Fe-based DMS. However, the large value of the spin-orbit coupling constant in Ni^{2+} will, most likely preclude significant Van Vleck paramagnetism. In addition, the electronic spectrum of Ni^{2+} in a T_d environment will be simpler than that of Fe^{2+} in view of the larger λ of the former. The limitations imposed by bulk crystal-growth techniques in the incorporation of transition-metal ions can be circumvented in techniques based on nonequilibrium growth, e.g., MBE; it is thus of interest to exploit Fourier transform spectroscopy in the study of MBE-grown DMS's such as $CdTe:Co^{2+}$, $CdTe:Cu^{2+}$, or $CdTe:Ni^{2+}$ or their CdSe counterparts.

ACKNOWLEDGMENT

The work reported in this paper was carried out with support from National Science Foundation Grant No. 89-21717.

[1]See, for example, J. K. Furdyna, J. Appl. Phys. **53**, 7637 (1982); **64**, R29 (1988).
[2]J. Lambe and C. Kikuchi, Phys. Rev. **119**, 1256 (1960).
[3]A. Twardowski, M. von Ortenberg, and M. Demianiuk, J. Cryst. Growth **72**, 401 (1985).
[4]B. T. Jonker, J. J. Krebs, S. B. Qadri, and G. A. Prinz, Appl. Phys. Lett. **50**, 848 (1987).
[5]B. T. Jonker, J. J. Krebs, and G. A. Prinz, Appl. Phys. Lett. **53**, 450 (1988).
[6]M. Villeret, S. Rodriguez, and E. Kartheuser, J. Appl. Phys. **67**, 4221 (1990).
[7]See, for example, W. Giriat and J. K. Furdyna, in *Diluted Magnetic Semiconductors,* Vol. 25 of Semiconductors and Semimetals, edited by J. K. Furdyna and J. Kossut (Academic, New York, 1988), p.1.
[8]BOMEM Inc., 450 Ave. St-Jean Baptiste, Quebec, Canada, G2E 5S5.
[9]M. K. Udo, Ph.D. thesis, Purdue University, 1991.
[10]Infrared Associates, Inc., 1002 Eastpark Boulevard, Cranbury, NJ 08512.
[11]Model 10DT supervaritemp optical cryostat, manufactured by Janis Research Company, Inc., 2 Jewel Drive, Wilmington, MA 01887-0896.
[12]This is the trade name for polycrystalline ZnS grown by chemical-vapor deposition, marketed by Janos Technology Inc., Rt. 35, Townshend, VT 05353.
[13]See, for example, A. Abragam and B. Bleaney, Electron Paramagnetic Resonance of Transition Ions (Clarendon, Oxford, 1970).
[14]M. Villeret, S. Rodriguez, and E. Kartheuser, Physica **B162**, 89 (1990). The wave functions are given in Tables 6 and 8 of this reference. Note that in Table 8 there are the following obvious misprints. The last term in ϵ_2'' should read $-5^{-1/2}|v_-,1\rangle$ and the wave functions $\delta_1'',\delta_2'',\delta_3''$ belong to Γ_4.
[15]M. Villeret, S. Rodriguez, and E. Kartheuser, Phys. Rev. B **43**, 3443 (1991); Solid State Commun. **75**, 21 (1990).
[16]M. Villeret, S. Rodriguez, and E. Kartheuser (unpublished).
[17]H. J. M. Swagten, A. Twardowski, W. J. M. de Jonge, and M. Demianiuk, Phys. Rev. B **39**, 2568 (1989).
[18]G. A. Slack, F. S. Ham, and R. M. Chrenko, Phys. Rev. **152**, 376 (1966).
[19]G. A. Slack, S. Roberts, and J. T. Vallin, Phys. Rev. **187**, 511 (1969); J. M. Baranowski, J. W. Allen, and G. L. Pearson, *ibid.* **160**, 627 (1967).
[20]J. M. Rowe, R. M. Nicklow, D. L. Price, and K. Zanio, Phys. Rev. B **10**, 671 (1974).
[21]A. Mooradian and G. B. Wright, *Proceedings of the IX International Conference on the Physics of Semiconductors* (Nauka, Leningrad, 1968), p. 1020.
[22]D. L. Peterson, Ph.D. thesis, Purdue University, 1984.
[23]D. Scalbert, J. Cernogora, A. Mauger, C. Benoit a la Guilaume, and A. Mycielski, Solid State Commun. **69**, 453 (1989).
[24]E. B. Wilson, J. C. Decius, and P. C. Cross, *Molecular Vibrations* (Dover, New York, 1980).
[25]E.-K. Suh, A. K. Arora, A. K. Ramdas, and S. Rodriguez, Phys. Rev. B **45**, 3360 (1992).
[26]R. Beserman, Solid State Commun. **23**, 323 (1977).